Journal of Alloys and Compounds 509 (2011) 27–32

Contents lists available at ScienceDirect

Journal of Alloys and Compounds

journal homepage: www.elsevier.com/locate/jallcom

Development of nano-structure Cu–Zr alloys by the mechanical alloying process

M. Azimi*, G.H. Akbari

Department of Material Science and Engineering, Shahid Bahonar University of Kerman, 76135-133, Kerman, Iran

ARTICLE INFO

Article history:
Received 10 May 2010
Received in revised form 16 July 2010
Accepted 19 August 2010

Keywords:
Nano-structured materials
Mechanical alloying
Crystal structure
X-ray diffraction

ABSTRACT

Cu–Zr alloys have many applications in electrical and welding industries for their high strength and high electrical and thermal conductivities. These alloys are among age-hardenable alloys with capability of having nano-structure with high solute contents obtainable by the mechanical alloying process. In the present work, Cu–Zr alloys have been developed by the mechanical alloying process. Pure copper powders with different amounts of 1, 3 and 6 wt% of commercial pure zirconium powders were mixed. The powder mixtures were milled in a planetary ball mill for different milling times of 4, 12, 48 and 96 h. Ball mill velocity was 250 rpm and ball to powder weight ratio was 10:1. Ethanol was used as process control agent (PCA). The milling atmosphere was protected by argon gas to prevent the oxidation of powders. The milled powders were analysed by XRD technique and were also investigated by SEM observations. Lattice parameters, crystal sizes and internal strains were calculated using XRD data and Williamson–Hall equation. Results showed that the lattice parameter of copper increased with increasing milling time. The microstructure of milled powder particles became finer at longer milling time towards nano-scale structure. SEM observations showed that powder particles took plate-like shapes. Their average size increased initially and reached a maximum value then it decreased at longer milling times. Different zirconium contents had interesting effects on the behavior of powder mixtures during milling.

1. Introduction

Alloys from low solubility systems are obtainable by either rapid solidification or mechanical alloying methods [1,2]. The advantages of mechanical alloying are higher solute contents more than equilibrium solubility limit and more homogeneous structure which are obtainable by high energy collisions between balls and powder particles during milling [2–4]. The equilibrium phase diagram of Cu–Zr system, Fig. 1, shows a very limited solubility of Zr in Cu. The maximum solubility at eutectic temperature is 0.172 wt% (0.0012 mole fraction) [6]. The solubility of Zr in Cu decreases with decreasing temperature so that these alloys are among age-hardenable alloys [7]. Their suitable cost with high wear [8] and corrosion resistance [9] have made these alloys suitable for vast applications in resistance welding technique and thermal–electrical components [10,11]. The equilibrium Cu–Zr phase diagram, Fig. 1, shows complete solubility in the liquid state. Therefore, it is possible to get a supersaturated solid solution by mechanical alloying method in the system [3].

Zr affects the stacking fault energy (SFE) and stacking fault probability (SFP) in copper. Because of the different crystal systems of Zr (hcp) and Cu (fcc), those effects are remarkable. It was reported that a little amount of Zr in triple alloy of CuCrZr was very effective in changing SFE. The effects were observed in TEM observations of stacking fault regions with partial dislocations [12]. The presence of Zr in Cu leads to the increasing of stacking fault regions, with high activation energy for reconciliation of partial dislocations which prevent cross slip of dislocations and delay in dynamic recovery. This is the reason for higher work hardening rate in Cu–Zr alloys than pure copper. In a reported work, Batra et al. [13] concluded that Zr in a triple alloy of CuCrZr increased the twinning and stacking fault regions in TEM observations. They attributed them to the decreasing effect of Zr on SFE of Cu which leads to a delay in dynamic recovery. This, in turn, leads to the increase of free energy of the system and facilitates the dynamic recrystallization process. Kalinin et al. [14] reported the effect of Zr on hardness peak in ageing process and recrystallization temperature of Cu.

In the present work, supersaturated Cu–Zr alloys with nano-structures were developed by mechanical alloying method and the characteristics of resulted powders were investigated.

2. Experimental procedure

2.1. Materials and mechanical alloying process

Copper electrolytic powders with the purity of 99.7% and particle sizes of less than 6 μm and zirconium powders with 97% purity and particle sizes of less than 9 microns were mixed with different ratios of 1, 3 and 6 weight percents of Zr. The powder mixtures were milled in a planetary palversity ball mill with high chromium stainless steel vial. Ball to powder weight ratio was 10:1. High chromium tempered

* Corresponding author. Tel.: +98 914 4916071; fax: +98 491 2258917.
E-mail address: mnr2_azimi@yahoo.com (M. Azimi).

0925-8388/$ – see front matter © 2010 Elsevier B.V. All rights reserved.
doi:10.1016/j.jallcom.2010.08.071

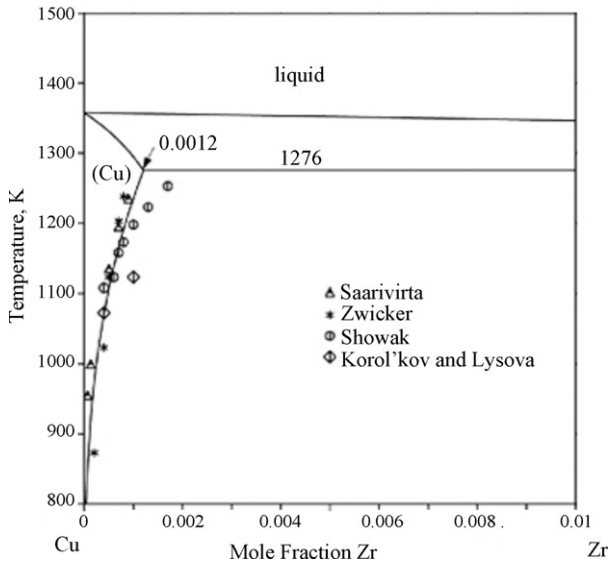

Fig. 1. Cu–Zr phase diagram in copper-riched zone [5].

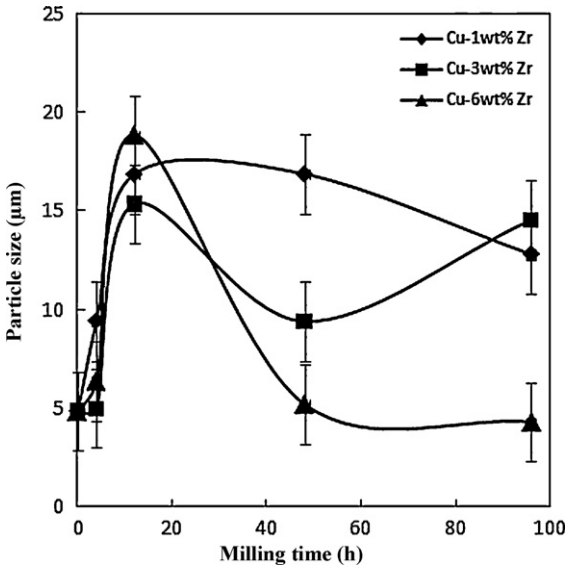

Fig. 2. The Variations of powder particle average sizes versus milling time in Cu–1,3,6 wt% Zr powder mixtures.

stainless steel balls in two sizes of 1 and 2 cm in diameter were used. Different ball sizes with their more accidental collisions [15] give more energy to powder particles [16] and also it gives rise to less adhesion of powders on ball surfaces and more homogeneity of product mixtures [17]. The powders were mixed half an hour in the mill without balls before milling. The milling process was carried out for different times of 4, 12, 48 and 96 h for all powder mixtures. Ethanol was used as PCA. The mill atmosphere was protected by argon gas to prevent the oxidation of powder particles. To control and prevent of temperature rise, 30 min stop was applied after every hour of milling. The velocity of ball mill was 250 rpm for all powder mixtures and milling times.

2.2. SEM observations and XRD analysis

The morphology of powder particles and their sizes were investigated by scanning electron microscope (SEM) CamScan MV2300 equipped with EDS analysis. The particle size characteristics were studied by Image Analyzer software. The milled powder mixtures were analysed by XRD-Philips X'pert with CuKα radiation. Lattice parameters were determined by the separation of $k\alpha_1$ and $k\alpha_2$ diffractions at high angles of (4 0 0), (3 3 1) and (4 2 0) with extrapolation function method. The measured lattice parameters were plotted versus $\cos\theta \times \cot\theta$ and the best fit with least square deviation was obtained. The cross point of the obtained line with vertical axis gives the best value for lattice parameter. Crystal sizes and internal strain were obtained by low angle diffractions of (1 1 1), (2 0 0) and (2 2 0) using Williamson–Hall equation as follows [18,19]:

$$\beta_r \cos\theta = \frac{k\lambda}{L} + 2\varepsilon \sin\theta$$

where ε is internal strain, β_r is peak broadening due to crystal refining and internal strain. The Scherrer constant, k, is 0.9 and $\lambda = 0.1541874$ nm. The plot of XRD peaks with the four variable Gaussian function was obtained and β_r was calculated by the equation $\beta_r^2 = \beta_0^2 - \beta_i^2$. β_i and β_0 are peak broadening from the instrument and total peak broadening, respectively. With the plotting of Williamson–Hall function crystal size, L, from the cross point and internal strain from the slope of the plotted line are obtainable.

As milled powder particles were cold-pressed in a plate shape die with 2 mm height. The compacted samples were polished by abrasive paper of number 5000 then by fine diamond paste of 1 and 0.25 μm. The Strueres microhardness tester Duramin20 was used to measure microhardness variations of powder particles during the milling process according to ASTM E 384-89 standard. The test was done by maximum load of 98.7 mN for 5 s. Indentations were carefully made onto polished particle surfaces and porosity areas were avoided to be ensured of the microhardness measurement results. The microstructures of powder particles were also investigated by optical microscope.

3. Results and discussion

3.1. Particle sizes and morphology

Figs. 2 and 3 illustrate the variations of particle sizes during milling. The particle sizes initially increase, reach maximum points and show decreasing trends at longer milling times. Powder mixtures with higher Zr contents, however, show higher decreasing rates which is significant for powder mixture with 6 wt% Zr.

The changes in morphology and size of particles in the powder mixture of Cu–6 wt% Zr are shown in Fig. 4. Particles become plate-like with increasing milling time and their sizes decrease evidently which are consistent with particle sizes in Fig. 2 against milling time. At the beginning of milling process, particles are soft and they are deformed due to high energy collisions of balls to particles, leading to microforging of powder particles. At this stage cold welding is the dominant process giving rise to increasing the average particle size and flattening of particles. At longer milling time, work hardening of particles renders them brittle and fracturing process becomes significant and the decreasing trend of particle sizes is observed. The presence of Zr in Cu matrix facilitates fracturing process of particles in two ways. Increasing of dissolved Zr atoms in the Cu matrix and increasing work hardening rate and promoting fracturing of Cu particles [20]. The other way is entrapment of Zr particles between Cu particles during ball-particle collisions. HCP Zr particles are more brittle than ductile FCC Cu particles. During milling and subsequent collisions between balls and mixed particles of Cu and Zr, in Zr parts with less ductility, cracks initiate and propagate more rapidly which can propagate into Cu parts and fracture Cu particles.

The increase of average particle size after 48 h milling, as evident in Figs. 2 and 5, may be attributed to some recovery and/or recrystallization effects due to high accumulated work hardening effects and temperature rise.

The EDS analysis of powder particles in Cu–6 wt% Zr milled for 96 h showed some Fe contamination as seen in Fig. 6. Iron particles entered in powder mixtures by wearing effects between balls and mill container wall. Iron atoms diffuse into copper matrix because of local high temperature surfaces of particles during milling operation. This contamination is more evident at longer milling times and in mixtures with higher Zr contents. It is attributed to finer particles which provide more surfaces for more diffusion of Fe atoms. The maximum iron content was 0.2 wt% in samples milled for 96 h. For those samples which were milled for shorter times, the iron contents were not significant. Therefore, the iron contamination effect was not considered in the results.

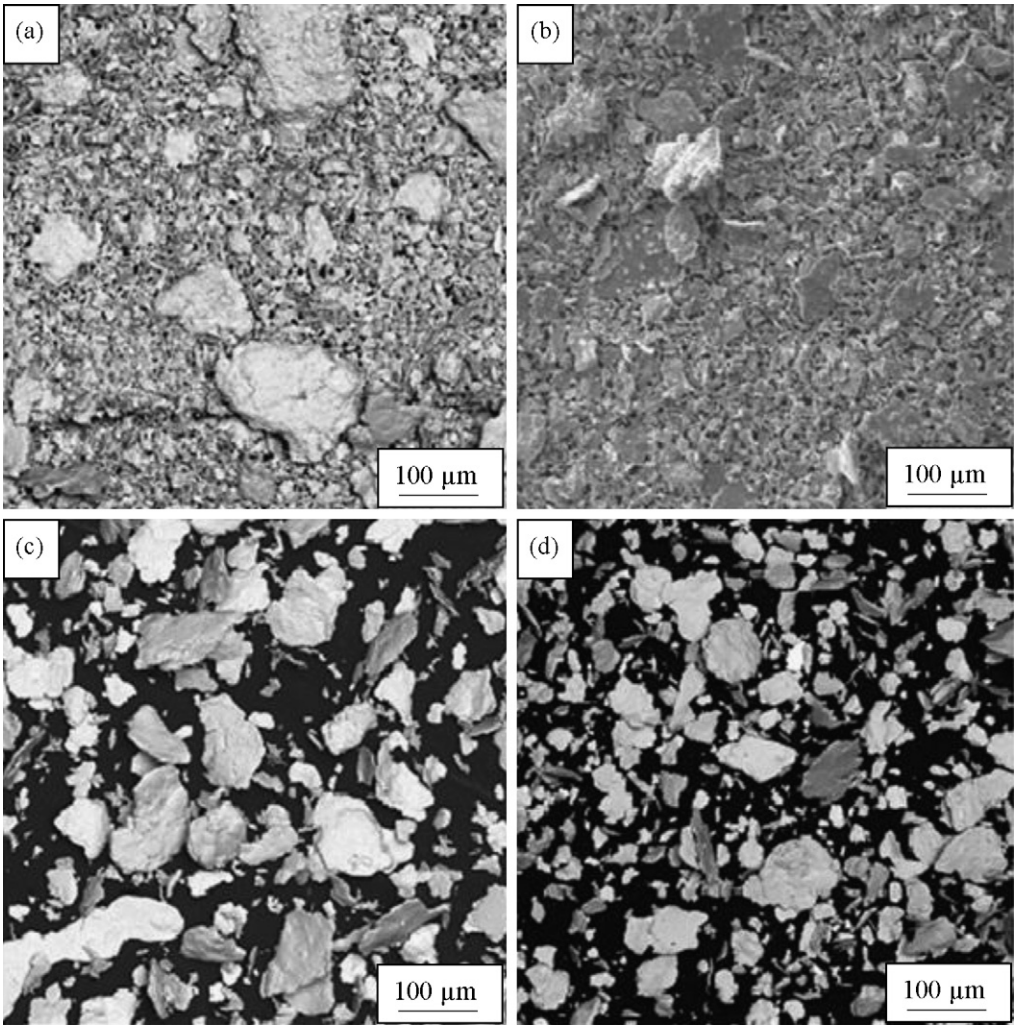

Fig. 3. The Influence of Zr content on powder particle size. (a) Cu–1 wt% Zr and (b) Cu–3 wt% Zr powder mixtures after 4 h milling, (c) Cu–1 wt% Zr and (d) Cu–3 wt% Zr powder mixtures after 48 h milling.

3.2. Lattice parameter

The variations of Cu lattice parameter in powder mixtures with 1, 3 and 6 wt% Zr against milling time are illustrated in Fig. 7. In all cases, lattice parameter increases with milling time. It suggests that solute zirconium content increases with increasing milling times. During milling and cold working of particles due to ball to particle collisions tremendous crystal defects such as vacancies, dislocations and sub-boundaries are created which provide suitable diffusion paths for Zr atoms [3,21]. Zr atoms mainly diffuse with vacancy mechanism. The bigger size of Zr atoms may lead to absorb vacancies more effectively [21]. Atom-pumping mechanism, which was suggested by Schwarz [22], may be operative in the Cu–Zr system. In atom-pumping mechanism the dislocation nucleus acts as a pump for solute atom. Since Zr atoms are bigger than Cu atoms, the lattice regions around Zr atoms become more compacted and more dislocations are developed at these areas. Namely, Zr atoms interact increasingly with dislocations and therefore dislocations facilitate diffusion of Zr atoms. The same conclusions were reported by Arnberg [7] and Liu [11] on the role of dislocations in supersaturated solid solution of Cu–Zr alloys. From the diagram, it is evident that higher Zr content in the initial mixture leads to higher lattice parameter of Cu matrix after the same milling time. More zirconium particles in the mixture lead to steeper concentration gradient of Zr atoms in Cu matrix and more diffusion of Zr atoms into Cu crystal and expansion of it. This is the reason for higher supersaturated solid solution of Zr in Cu matrix with higher Zr content of initial powder mixture.

In the sample with 3 wt% Zr a different trend at longer milling is observed. The lattice parameter has strangely decreased to the almost pure copper crystal. An unusual result is also observed in Fig. 2. The average particle size for Cu–3 wt% Zr has increased at longer milling time of 96 h. The same particles are shown in Fig. 5c. They are relatively coarse agglomerated particles. Microhardness measurements show consistency with this abnormality, with lower hardness of the same sample after 96 h milling compare to that sample milled after 48 h as seen in Fig. 8. Fig. 9 illustrates the optical micrographs of Cu–3 wt% Zr samples milled for 48 and 96 h. In Fig. 9a, after 48 h of milling, cold-worked structure areas together with some recrystallized areas are clearly observed. It is evident that cold-worked structure is developed during milling as a result of ball-powder particle collisions. In Fig. 9b, the sample after 96 h of milling, recrystallized and unrecrystallized areas are observed. But the hardness of unrecrystallized areas is slightly lower than that of unrecrystallized areas in the sample which was milled for 48 h. The observation of recrystallized areas, coarse particles with reduction of lattice parameter, Fig. 7, suggest that because of temperature rise, some recovery and recrystallization processes have taken place and at the same time some of supersaturated dissolved Zr atoms have come out of solution leading to decrease of Cu lattice parameter.

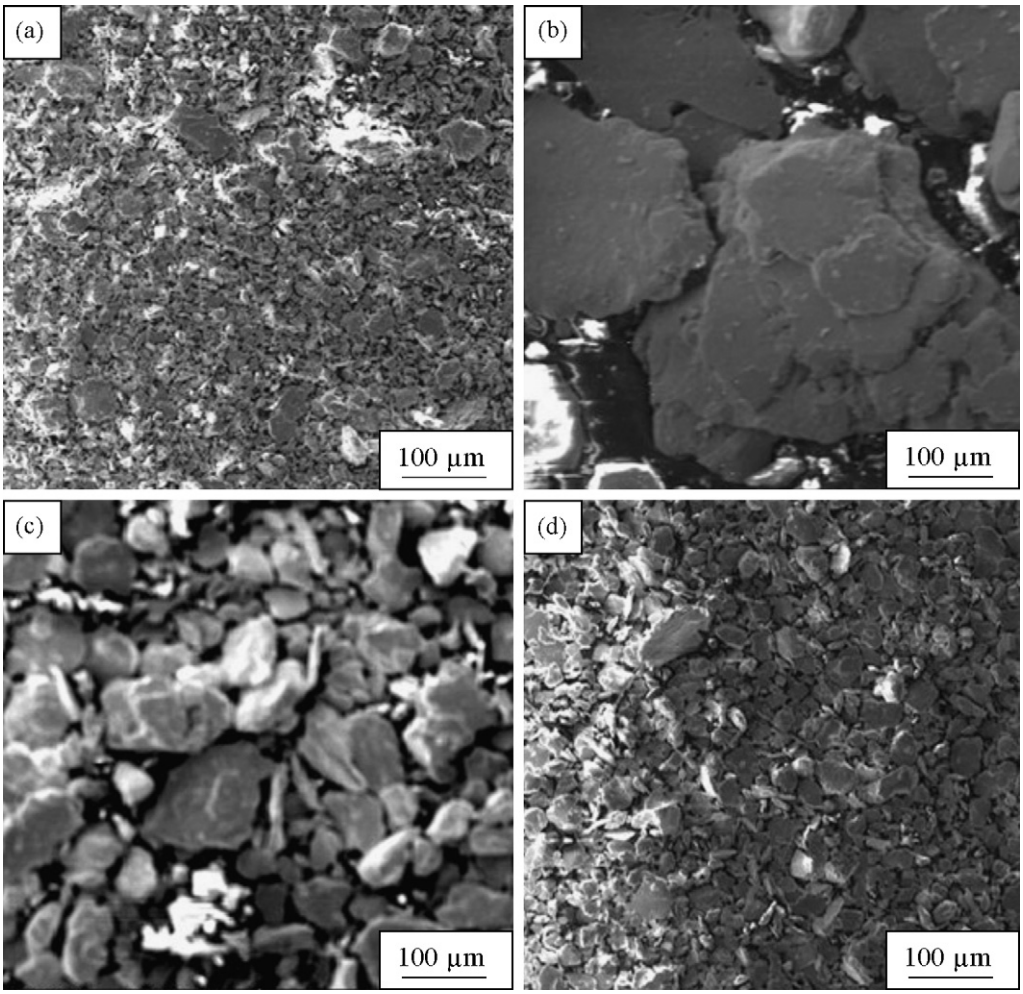

Fig. 4. The Effect of milling time on particle morphology in Cu–6 wt% Zr. (a) 4, (b) 12, (c) 48 and (d) 96 h.

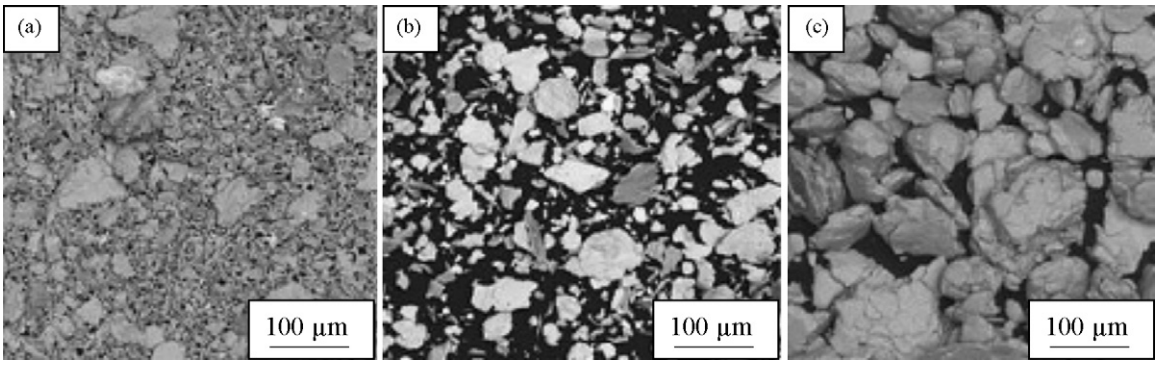

Fig. 5. Particle sizes in Cu–3 wt% Zr after different milling times. (a) 4, (b) 48, (c) 96 h.

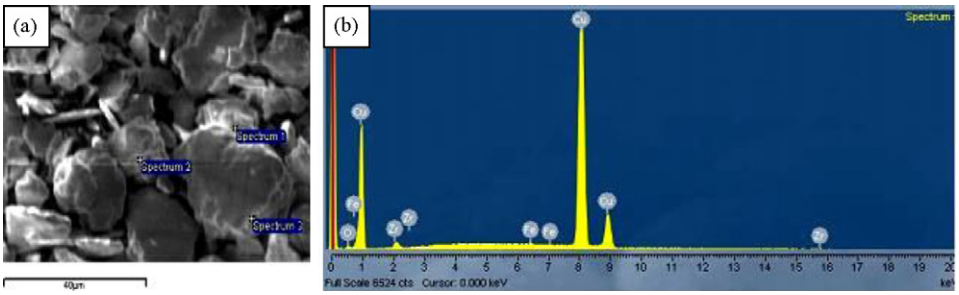

Fig. 6. a) SEM micrograph of powder particles in Cu–6 wt% Zr after 96 h milling, b) EDS analysis in spectrum1.

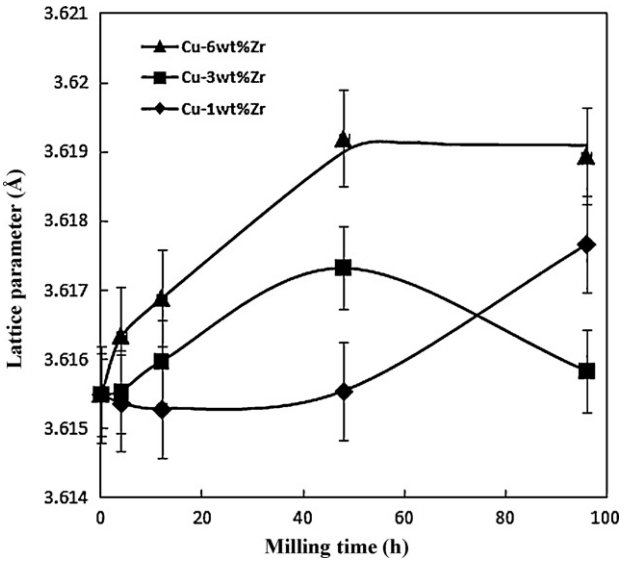

Fig. 7. Cu lattice parameter variations versus milling time in Cu–1,3,6 wt% Zr powder mixtures.

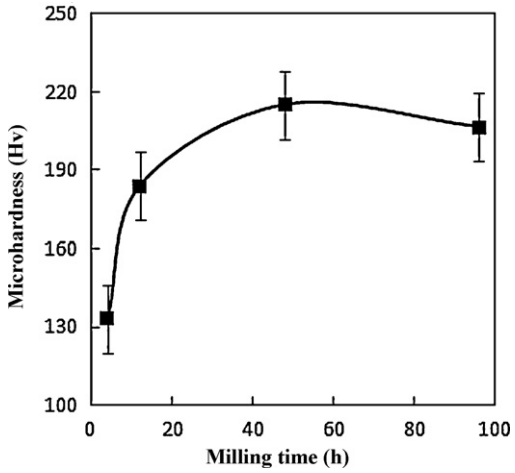

Fig. 8. Microhardness variations during milling in Cu–3 wt% Zr powder mixture.

3.3. Crystal size and internal strain

The variations of crystal sizes in the three samples of 1, 3 and 6 wt% Zr contents during milling are given in Fig. 10. According to the figure, after 12 h of milling in all samples crystal sizes are in the range of 33 to 97 nm. During milling, powder particles are subjected to severe plastic deformation, which results in multiplication and increase of dislocation density in copper matrix. At the same time temperature may rise locally and especially at particle surfaces enough for diffusion of Zr atoms into Cu matrix. Dislocation networks are suitable paths for high diffusion rates for Zr atoms. But more plastic deformation in pre-cold-worked matrix may move dislocations without moving diffused Zr atoms in them. Therefore Zr atoms may be left inside Cu matrix. Repeating this process by continuing milling operation will lead to a more homogeneous distribution of dissolved Zr atoms with much higher concentration than the equilibrium value. At longer milling times, higher dislocation densities and their pile-ups at obstacles may lead to the formation of new boundaries and fragmentation of initial crystals into nano-scale crystals. Formation of nanocrystals and diffusion of Zr atoms into Cu matrix will continue even more rapidly since more boundaries facilitate the diffusion process.

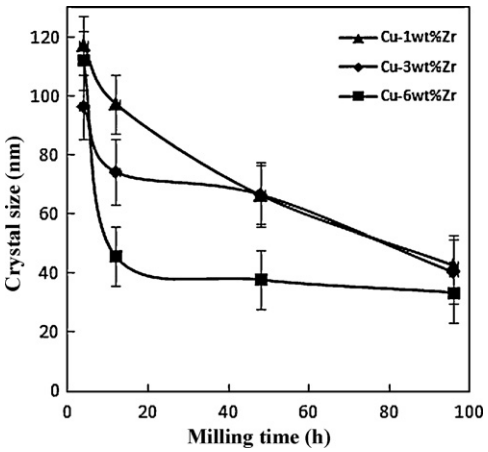

Fig. 10. Crystal size variations during milling in Cu–1,3,6 wt% Zr powder mixtures.

The effect of Zr content in initial powder mixtures on the above-mentioned processes is evident from the data in Fig. 10. Higher Zr contents result in smaller crystal sizes during milling. Zr has a very limited solubility in copper matrix. Zr particles with HCP crystal system are much more brittle than Cu particles. Therefore Zr particles are broken during milling and become finer with increasing of milling time. The fine broken Zr particles are randomly distributed between cold-worked Cu particles and provide suitable conditions for diffusion as mentioned in the above section. Harder Zr particles between Cu particles may help to cold work effect on the Cu parti-

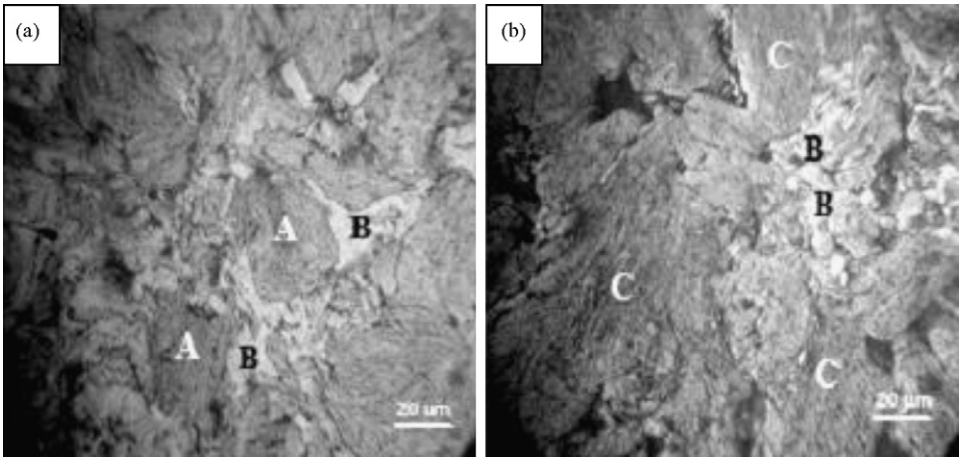

Fig. 9. Microstructures of particles in Cu–3 wt% Zr powder mixture milled for (a) 48 and (b) 96 h. (A) cold-worked areas, (B) recrystallized areas, and (C) recovered areas.

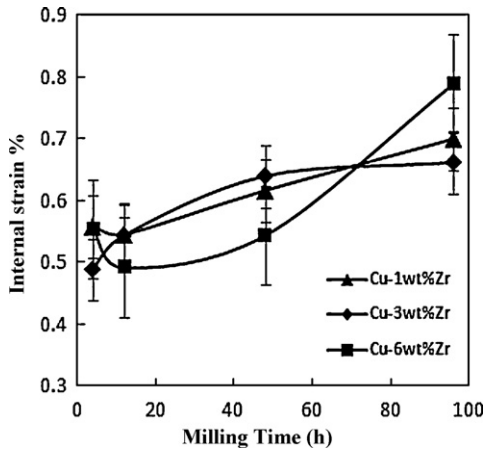

Fig. 11. Internal strain variations during milling in Cu–1,3,6 wt% Zr powder mixtures.

cles. It can be concluded that higher initial contents of Zr facilitate all above processes and therefore increase the dissolved Zr atoms in the matrix and work hardening rate of Cu matrix. They also may strongly affect subsequent restoration processes after cold working which may take place locally during milling or annealing processes afterwards if they are applied on the milled products.

Fig. 11 gives internal strain against milling time in powder mixtures with 1, 3 and 6 wt% Zr. As expected, internal strain increases with increasing of milling time more rapidly at the beginning and with slower trend at longer milling times. Internal strain variations seem normal behavior, which are resulted from cold working effects. Cold working features such as vacancies, dislocations and stacking faults are created and increased due to ball-particle-ball or ball-particle-container wall collisions. Their increasing trend will slow down with increasing of milling time for samples with 3 wt% Zr but for 1 and 6 wt% Zr samples, slowing down trend is not observed at longer milling times. It is worthy to mention that the presence of Zr particles and dissolving of Zr atoms in Cu matrix facilitate cold working effects and consequently internal strains. However, accumulation of cold working effects leads to the saturation of cold-worked matrix and slowing down the increase rate of internal strains at longer milling times. Solute Zr atoms decrease the stacking fault energy of Cu crystal. This may lead to less recovery process in cold-worked Cu particles and consequently the lack of slowing down trend in samples with 1 and 6 wt% Zr as mentioned above.

4. Conclusions

1. It is possible to obtain nano-scale crystal size in Cu–Zr alloys by the mechanical alloying process.
2. After 12 h of milling operation crystal sizes in the range of 33–97 nm were obtained.
3. Increasing of Zr content in initial powder mixtures facilitates nano-structure development in Cu–Zr powder mixtures.
4. Mechanical alloying is an effective technique to obtain supersaturated Cu–Zr solid solutions with Zr contents much higher than the equilibrium value.

References

[1] A.N. Patel, S. Diamond, J. Mater. Sci. Eng. 98 (1988) 329–334.
[2] E. Botcharova, M. Heilmaier, J. Freudenberger, et al., J. Alloys Compd. 351 (2003) 119–125.
[3] C. Suryanarayana, Mechanical Alloying and Milling, first ed., Marcel Dekker, New York, 2004.
[4] P.A. Rojas, A. Peñaloza, C.H. Wörner, et al., J. Alloys Compd. 425 (2006) 334–338.
[5] N. Wang, Ch. Li, Zh. Du, F. Wang, W. Zhang, J. Comput. Coupling Phase Diagrams Thermochem. 30 (2006) 461–469.
[6] ASM International Handbook Committee, Metals Handbook, vol. 3, Metals Park, Ohio, 1992.
[7] L. Arnberg, U. Backmark, N. Backstrom, J. Lange, J. Mater. Sci. Eng. 83 (1986) 115–121.
[8] J.P. Tu, W.X. Qi, Y.Z. Yang, et al., J. Wear 249 (2002) 1021–1027.
[9] Z. Li, J. Shen, F. Cao, Q. Li, J. Mater. Proc. Tech. 137 (2003) 60–64.
[10] M. Xie, J. Liu, X. Lu, et al., J. Mater. Sci. Eng. A 304–306 (2001) 529–533.
[11] P. Liu, B.X. Kang, X.G. Cao, et al., J. Mater. Sci. Eng. A 265 (1999) 262–267.
[12] K. Kapoor, D. Lahiri, I.S. Batra, et al., J. Mater. Charact. 54 (2005) 131–140.
[13] I.S. Batra, et al., J. Nucl. Mater. 299 (2001) 91–100.
[14] G. Kalinin, V. Barabash, A. Cardella, et al., J. Nucl. Mater. 10 (2000) 283–287.
[15] L. Takacs, C. Suryanarayana,et al., Processing and Properties of Nanocrystalline Materials, Warrendale, 1996.
[16] D. Gavrilov, O. Vinogradov, W.J.D. Shaw, Proc. of Inter. Confer. on Composite Mat., ICCM-10, vol. 3, Canada, Woodhead Publishing, 1995, p. 11.
[17] L. Takacs, M. Pardavi-Horvath, J. Appl. Phys. 75 (1994) 5864–5866.
[18] B.D. Cullity, Elements of X-Ray Diffraction, Addison-Wesley Publishing Company, 1978.
[19] G.K. Williamson, W.H. Hall, J. Acta Metall. 1 (1953) 22–31.
[20] ASM International Handbook Committee, Metals Handbook, vol. 2, tenth ed., Metals Park, Ohio, 1993.
[21] D.A. Porter, K.E. Easterling, Phase Transformations in Metals and Alloys, second ed., Chapman & Hall, London, 1992.
[22] R.B. Schwarz, J. Mat. Sci. Forum. 269–272 (1998) 665–674.